Journal of University of Science and Technology Beijing
Volume 10, Number 4, August 2003, Page 55

Computer simulation of strain-induced morphological transformation of coherent precipitates

Yuhong Zhao, Zheng Chen, and Xiaoling Li

Department of Materials Science and Engineering, Northwestern Polytechnical University, Xi'an 710072, China

(Received 2002-05-28)

Abstract: The coherent elastic strain-induced morphological transformation of a binary cubic model alloy was simulated with different strain energy parameters. The microscopic diffusion equation was combined with the theory of microscopic elasticity. The results show that when the strain energy is neglected, the randomly distributed equiaxed particles are obtained with isotropic characteristic. It is coarsening that follows the Ostwald ripening mechanism: smaller particles dwindle and larger particles grow; when the elastic strain is considered, plate precipitates tend to align along the elastically soft directions <01> with anisotropic characteristic. The particles grow in the soft directions and coarsen further; particles dwindle in out of the soft directions. While the coarsening of the particles localized in the same row or column follows the rule: smaller particles shrink and larger ones grow.

Key words: elastic strain energy, coherent precipitate, model alloy and computer simulation

[*This work was sponsored by the National Natural Science Foundation of China (No.50071046).*]

1 Introduction

During the diffusion process of aging alloys, if the rearrangements of atoms result in different lattice parameters between coherent precipitates and matrix phases, then there exist elastic strain fields around precipitates, and their superposition result in long-range elastic interactions, which dramatically affect the shapes and spatial arrangement of precipitate particles. Many experiments have been carried out on the dynamic mechanism of aging alloys [1, 2], yet the work of computer simulation is still at it's initial stage, and is only focused on the system without elastic strain energy [3, 4].

In this paper, based on the microscopic diffusion equation and microscopic elasticity theory, the computer simulation of coherent strain-induced morphological transformation of binary cubic model alloy is performed. In this model, the only input needed is the information concerning interaction potentials. The model can describe simultaneously very different structural transformations, such as shapes, habits, mutual distributions and concentration profiles *etc.* within the same formalism. Any a priori assumptions concerning the above information become unnecessary.

2 Theory and method

2.1 Microscopic diffusion equation

The diffusion relaxation of atoms between lattice sites is described by the Önsager equation [5]:

$$\frac{\mathrm{d}n(\vec{r},t)}{\mathrm{d}t}=\frac{C(1-C)}{k_{\mathrm{B}}T}\sum_{\vec{r}'}L_0(\vec{r}-\vec{r}')\frac{\delta F}{\delta n(\vec{r}',t)} \tag{1}$$

The function $n(\vec{r},t)$ characterizes a single occupation probability on the site $\vec{r}$ at time t, it can describe the morphology of precipitate. $L(\vec{r}-\vec{r}')$ is a constant matrix related to the probabilities of elementary diffusion jumps from lattice $\vec{r}$ to $\vec{r}'$, T the thermodynamic temperature, k_{B} the Boltzmann' s constant, C the average alloy composition, F the total Gibbs free energy of the system.

The Fourier transform of equation (1) is:

$$\frac{\mathrm{d}\tilde{n}(\vec{k},t)}{\mathrm{d}t}=\frac{C(1-C)}{k_{\mathrm{B}}T}\tilde{L}_0(\vec{k})\left\{\frac{\delta F}{\delta n(\vec{r},t)}\right\}_{\vec{k}} \tag{2}$$

where $\vec{k}$ is the reciprocal lattice vector within the first Brillouin zone. $\tilde{n}(\vec{k},t)$, $\tilde{L}_0(\vec{k})$ and $\left\{\frac{\delta F}{\delta n(\vec{r},t)}\right\}_{\vec{k}}$ are the Fourier transforms of $n(\vec{r},t)$, $L_0(\vec{r}-\vec{r}')$ and

Corresponding author: Yuhong Zhao, **E-mail:** zyh388@sina.com

$\frac{\delta F}{\delta n(\vec{r},t)}$, respectively.

In the mean-field approximation [6], the free energy in equation (1) is given by:

$$F=\frac{1}{2}\sum_{\vec{r}}\sum_{\vec{r}'}W(\vec{r}-\vec{r}')n(\vec{r})n(\vec{r}')+ k_BT\sum_{\vec{r}}[n(\vec{r})\ln n(\vec{r})+(1-n(\vec{r}))\ln(1-n(\vec{r}))] \quad (3)$$

where $W(\vec{r}-\vec{r}')$ is a pairwise interaction energy between two atoms at lattice sites $\vec{r}$ and $\vec{r}'$, including chemical and elastic interactions:

$$W(\vec{r}-\vec{r}')=W(\vec{r}-\vec{r}')_f+W(\vec{r}-\vec{r}')_{el} \quad (4)$$

2.2 Microscopic elasticity theory

In the microscopic elasticity theory, the strain energy of a binary solid solution is given as a sum of two physically distinct terms [6]:

(1) The configuration-independent term: the self-energy and image force-induced energy.

(2) The configuration-dependent term: the energy from concentration inhomogeneity.

The first term is not affected by spatial redistribution of solute atoms and therefore it can be ignored. The second term gives a nonlocal strain energy change associated with spatial distribution of solute atoms, and affects the precipitate morphology. In the real space, it's given by:

$$E_{el}=\frac{1}{2}\sum_{\vec{r}\vec{r}'}W_{el}(\vec{r}-\vec{r}')n(\vec{r})n(\vec{r}') \quad (5)$$

The Fourier transform of equation (5) is [7]:

$$E_{el}=\frac{1}{2N}\sum_{\vec{k}}{}'V(\vec{k})_{el}|\tilde{n}(\vec{k})|^2 \quad (6)$$

where N is the total number of lattice sites. The prime in the summation (6) implies that the point $\vec{k}=0$ is excluded because $V(\vec{k})_{el}$ has a singularity at $\vec{k}=0$. $V(\vec{k})_{el}$ is the function of elastic energy density, it's the Fourier transform of $W(\vec{r})_{el}$, with the long-wave approximation [6] it can be written:

$$V(\vec{k})_{el}\approx B(\vec{e})=-\sigma_0^2[e_i\Omega(\vec{e})_{ij}e_j-<e_i\Omega(\vec{e})_{ij}e_j>_{\vec{e}}] \quad (7)$$

where $\sigma_0=(c_{11}+2c_{12})\varepsilon_0$, c_{11} and c_{12} are the elastic constants of a cubic crystals. Generally, solute atoms are dilatational centers and their introduction leads to an isotropic crystal lattice expansion characterized by a stress-free strain tensor $\varepsilon_{ij}^0=\varepsilon_0\delta_{ij}$, $\varepsilon_0=da/adc$ is the concentration coefficient of the crystal lattice expansion, a the crystal lattice parameter of the matrix, δ_{ij} the kronecker delta symbol, $\vec{e}=\vec{k}/k$ the unit vector in the $\vec{k}$ direction, $<\cdots>_{\vec{e}}$ the symbol of averaging over all directions $\vec{e}$, $\Omega(\vec{e})_{ij}$ the Green tensor reciprocal to $c_{ijkl}e_ke_l$.

2.3 The kinetic model

The Fourier transform of the variational derivative of (3) yields:

$$\left\{\frac{\delta F}{\delta n(\vec{r},t)}\right\}_{\vec{k}}=V(\vec{k})n(\vec{k},t)+k_BT\left\{\ln\frac{n(\vec{r},t)}{1-n(\vec{r},t)}\right\}_{\vec{k}} \quad (8)$$

$$V(\vec{k})=V(\vec{k})_f+B(\vec{e}) \quad (9)$$

Substituting (9) for (8) and (8) for (2), yields a reciprocal space representation of the kinetic equation:

$$\frac{d\tilde{n}(\vec{k},t)}{dt}=\frac{C(1-C)}{k_BT}\tilde{L}_0(\vec{k})\left\{[V(\vec{k})_f+B(\vec{e})]\tilde{n}(\vec{k},t)+k_BT\left[\ln\left(\frac{n(\vec{r},t)}{1-n(\vec{r},t)}\right)\right]_{\vec{k}}\right\} \quad (10)$$

Using a 2-neighbor interaction model [7], the function $V(k)_f$ can be written as:

$$V(\vec{k})_f=2w_1[\cos(k_xa)+\cos(k_ya)]+4w_2\cos(k_xa)\cos(k_ya) \quad (11)$$

$\vec{k}=(k_x,k_y)$, k_x and k_y are the components of vector $\vec{k}$ along the x and y axes parallel to the [10] and [01] directions in the reciprocal space; w_1 and w_2 are the nearest and next nearest neighbor pairwise interchange energies.

In the 2D-model [8] the elastic strain energy function $B(\vec{e})$ can be approximately written as

$$B(\vec{e})\approx B(e_x^2e_y^2-0.125) \quad (12)$$

$\vec{e}_x$ and $\vec{e}_y$ are the components of the unit vector $\vec{e}$ along the x and y axes in the reciprocal space, $B=-\frac{4(c_{11}+2c_{12})}{c_{11}(c_{11}+c_{12}+2c_{44})}\varepsilon_0^2\Delta$ is a material constant characterizing the elastic properties and the crystal lattice mismatch, $\Delta=c_{11}-c_{12}-2c_{44}$ is the elastic anisotropy constant [9].

According to the mean-field approximation, the minimizing free energy of the system when $n(\vec{r})\to c$ as follows:

$$F=N\left[\frac{1}{2}V(0)c^2+k_BT(c\ln c+(1-c)\ln(1-c))\right] \quad (13)$$

Since the function $B(\vec{e})$ has a singularity at

$\vec{k} \to 0$, the situation is complicated, while $\vec{e}_0 = <01>$ is the "soft" directions providing the minimum value of $B(\vec{e})$. According to equation (11), $B(\vec{e}_0) = -0.125B$, thus $V(\vec{k})_{\min} = V(0)_f + B(\vec{e}_0)$, then the free energy model resulting in the sable coherent diagram shown in **figure 1** is:

$$F = N\left[\frac{1}{2}(V(0)_f - 0.125B)c^2 + k_B T(c\ln c + (1-c)\ln(1-c))\right] \quad (14)$$

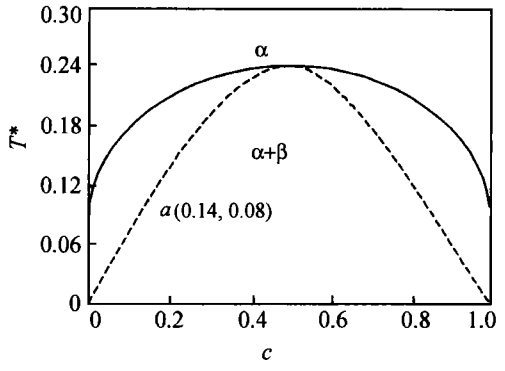

Figure 1 The equilibrium phase diagram of model alloy (*c*—content of the solute atom).

Using (11), (12) and (14) in (10) and introducing the reduced strain energy parameter $B^* = B/|V(0) - 0.125B|$, reduced temperature $T^* = k_B T/|V(0) - 0.125B|$, reduced time $t^* = t[L_1 c(1-c)/k_B T]\cdot|V(0) - 0.125B|$, thus the kinetic equation can be written in a dimensionless form:

$$\frac{d\tilde{n}(\vec{k},t^*)}{dt^*} = -2\{[(2-\cos(k_x a)-\cos(k_y a))+ \alpha(2-\cos(k_x a + k_y a)-\cos(k_x a - k_y a))]\times \left\{\left[\frac{2w_1(\cos k_x a + \cos k_y a)+ 4w_1/\sqrt{2}\cos(k_x a)\cos(k_y a)}{|V(0) - B/8|} + B^*(e_x^2 e_y^2 - 0.125)\right] + T^*\left[\ln\left(\frac{n(\vec{r},t^*)}{1-n(\vec{r},t^*)}\right)\right]\right\} \quad (15)$$

Equation (15) is good for any system with long-range interactions. The longer the interaction range, the more accurate the equation. It is especially accurate in the presence of long-range strain-induced interaction [10]. It is a nonlinear equation and a numerical solution would be preferred. The Euler method is utilized:

$$\tilde{n}(\vec{k},t^* + \Delta t^*) = \tilde{n}(\vec{k},t^*) + \frac{d\tilde{n}(\vec{k},t^*)}{dt^*}\Delta t^* \quad (16)$$

where Δt^* is a time increment.

3 Simulation results

In this paper, a binary substitutional alloy is considered. The phase diagram is shown in figure 1. Assuming that the two coherent phases have the same disordered structure and elastic modular, but different compositions, which result in different crystal lattice parameters. The 2D simulation is performed in a square lattice consisting of 128×128 unit cells, and periodic boundary conditions are applied.

An alloy with composition c =0.14 is aged at T^* =0.08, the corresponding point in figure 1 is point "*a*" denoting the homogeneous disordered solid solution and closing to the one side of the spinodal. Its initial condition is completely disordered with the occupation probability of solute atoms at each site defining average composition, small perturbations are added. When $B^* = 0.0$, the term of random noise is considered in the previous 1000 steps; while when $B^* = 1.25$, the steps needed are 3000 to induce the decomposition. The solution of equation (14) is carried out using the Euler method, $\tilde{n}(\vec{k},t)$ describes the concentration wave amplitudes within the entire first Brillouin zone, its back Fourier transform $n(\vec{k},t)$ gives the occupation probability, which is represented by a gray scale on which black indicates 0 and white 1.

The simulation results with strain energy parameter $B^* = 0.0$ are presented in **figure 2.** As shown in figure 2(a), at $t^* = 10$, the decomposition starts by developing concentration waves along all directions; at $t^* = 20$ (see figure 2(b)), some isolated axed precipitate particles are formed in the solute-lean dark matrix; at $t^* = 40$ (see figure 2(c)), randomly distributed isolated particles are formed completely; at $t^* = 100$ (see figure 2(d)), the coarsening of precipitates can be obviously observed.

The phase decomposition conditions with $B^* = 1.25$ are shown in **figure 3.** As shown in figure 3(a), when $t^* = 20$, at the initial stage of decomposition, fine and diffuse concentration modulations approximately along <01> "soft" directions developed first. The condition at $t^* = 30$ is demonstrated in figure 3(b), the precipitates particles are formed at nodes produced by intersections of the maxima of the two mutually perpendicular concentration modulations along the two directions, and they are linked by "gray linkage bridges". Figure 3(c) presents the state at $t^* = 80$, the nodes develop into plate-like particles tending to distribute along <01> directions by absorbing solute atoms from all connecting linkages. The state at $t^* = 160$ is shown in figure 3(d), the

coarsening of precipitates has taken place.

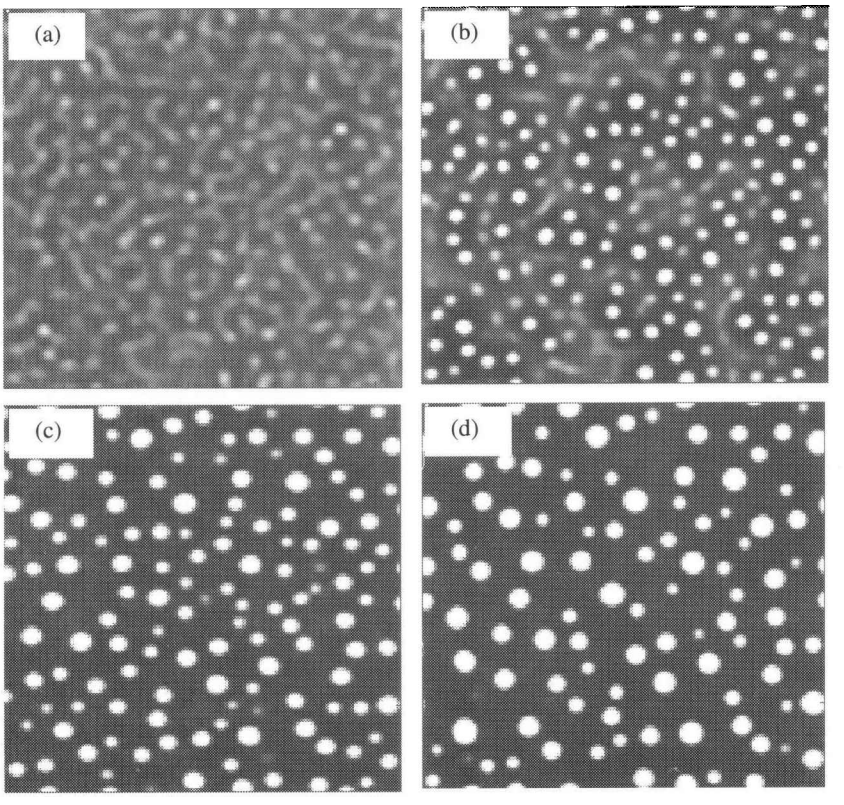

Figure 2 Computed microstructure for B^*=0.0 at various stages, (a) t^* = 10; (b) t^* = 20; (c) t^* = 40; (d) t^* = 100.

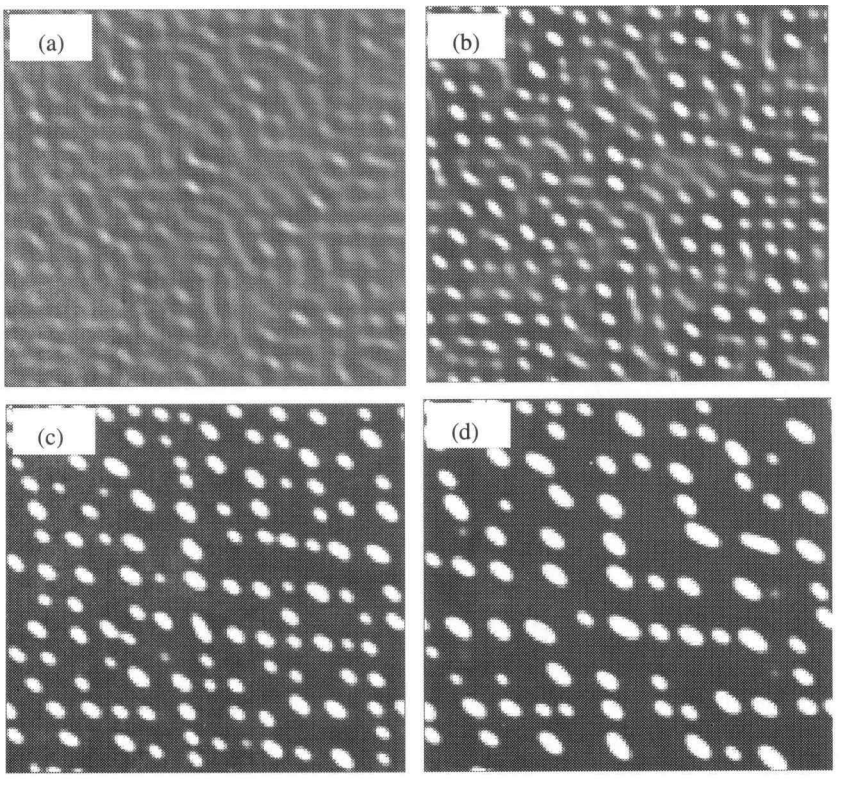

Figure 3 Computed microstructure for B^*=1.25 at various stages, (a) t^* = 20; (b) t^* = 30; (c) t^* = 80; (d) t^* = 160.

4 Analysis and discussions

It can be seen from figures 2 and 3 that the phase transformation is taken place by spinodal decomposition mechanism, which coincides with the phase diagram figure 1 of the model alloy: the representing point lies below the spinodal line.

As shown in figure 2, where $B^* = 0.0$, randomly

oriented concentration waves develop first, an highly interconnected "sponge-like" structure which is similar to that obtained in the symmetrical case [11] is predicted in the initial stage. The structure is unstable and the connectivity is broken immediately (figure 2(b)). The two phases develop toward their equilibrium state, at last the isolated equiaxed precipitates particles randomly distributed in the solute-lean dark matrix are formed. In this case, the elastic strain energy is neglected and the development is controlled only by the interfacial energy, whose reducing can provide the driving forces of phase transformation. Thus the sphere-like particles having the minimizing interfacial energy are formed. Upon further aging, we can clearly see the shrinkage of smaller particles and the growth of larger particles, which follows the Ostwald ripening theory. Therefore the interfacial energy decreases further. In order to provide the isotropic interfacial energy, the ratio of w_1 and w_2 is chosen to be $\sqrt{2}$. So the microstructure has an isotropic characteristic during the evolution process.

As $B^*=1.25$, both the strain energy and the interfacial energy control the transformation. Although the treatment of interfacial energy is the same as $B^*=0.0$, morphology here has a significant anisotropic characteristic. The reason is that the <01> directions are the elastic "soft" directions along which the strain energy of the cubic model alloy has the minimizing value in 2D case. In the Fourier space, the wave vectors along the elastic "soft" directions have bigger factors of increasing amplitudes, so the precipitate particles tend to arrange along them. If only the elastic strain energy is considered, plate-like precipitates are preferred and sphere particles are nearly impossible to form. Here the competition of the strain energy and the interfacial energy results in the formation of the ellipsoidal-plate-like precipitates. From figures 3(a) and 3(d), we can observe the selective growth and coarsening of precipitates. It follows that particles grow in the soft directions and coarsen further, particles dwindle in out of the soft directions, while the coarsening of the particles sitting in the same row or column follows the Ostwald ripening theory, smaller particles shrink and larger ones grow.

Comparing figures 2 and 3, it can be seen that the phase decompositions latter take place slower than the former. Therefore, it is thought that the coherent strain energy can decrease the effective driving force of spinodal decomposition. So, stronger concentration fluctuations are needed to stimulate spinodal decomposition.

The simulated result is compared with the experimental result [12] in **figure 4**. Figure 4(a) represents the simulated microstructure of 14% (atomic fraction, so as the follows) model alloy aged at $T^*=0.08$ for $t^*=160$. Figure 4(b) represents the TEM image of Ni-32.7%Cu-9.2%Si aged at 650℃ for 120 min observed by Tyapkin *et al.* The simulated microstructure shown in figure 4(a) is in good agreement with the observation by Tyapkin *et al.* in Ni-Cu-Si alloys. Both of them have the selective growth and coarsening characteristic. Furthermore, some square precipitate macrolattices are found in the two cases. The regardless of its oversimplification, the model can be efficiently used in many cases for understanding, interpreting and predicting structural evolution in real alloys.

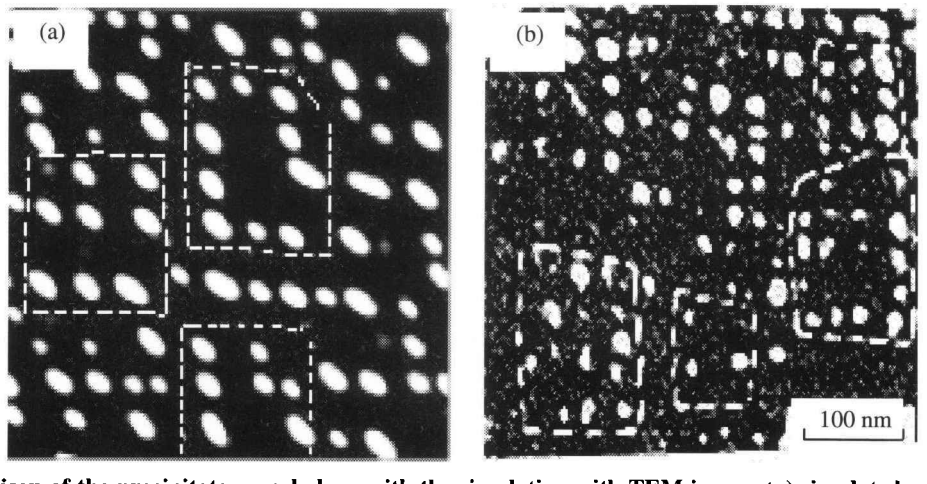

Figure 4 Comparison of the precipitate morphology with the simulation with TEM image, (a) simulated microstructure of 14% model alloy, T^*=0.08, t^*=160, aging; (b) TEM image of Ni-32.7%Cu-9.2%Si (atomic fraction) aged at 650℃ for 120 min.

5 Conclusions

(1) With $B^*=0.0$, the randomly distributed equiaxed precipitate particles are formed. The microstructure has an isotropic characteristic; its coarsening process follows the Ostwald ripening theory: smaller

particles dwindle and larger particles grow.

(2) With $B^* = 1.25$, the ellipsoidal-plate-like precipitates are formed and tend to arrange along the <01> directions. The morphology has an anisotropic characteristic. The growth and coarsening of precipitates follow the selective law, and particles grow in the preferring directions and coarsen further, particles dwindle in out of the soft directions. While the coarsening of the particles sitting in the same row or column follows the rule: smaller particles shrink and larger ones grow.

References

[1] Z. Chen, Y.X. Wang, B. Liu, *et al.*, Influence mechanism of Cerium on the threshold of short fatigue crack for Al-Li alloy 2090 [J], *Rare Met.*, 20(2001), No.1, p.31.

[2] Y.D. Tyapkin and Y.I. Maliyenko, Rearrangement of regular distributions during Ostwald coalescence of Fe-Be alloys [J], *Phys. Met. Metall*, 68(1989), No.4, p.125.

[3] X.L. Li, B. Liu, Z. Chen, *et al.*, Computer simulation of nucleation mechanism of δ' phase of Al-Li alloy [J], *Rare Met. Mater. Eng.* (in Chinese),31(2002), No.2, p.110.

[4] X.L. Li, Z. Chen, and B. Liu, Transition from metastability to Instability in the Dynamics for the precipitation of δ' (Al_3Li) [J], *Rare Met.*, 20(2001), No.4, p.240.

[5] Y. Wang, L.Q. Chen, and A.G. Khachaturyan, Kinetics of strain-induced morphological transformation in cubic alloys with a miscibility gap [J], *Acta Metall. Mater.*, 41(1993), No.1, p.279.

[6] G. Khachaturyan, *Theory of Structural Transformation in Solids* [M], Wiley, New York, 1983, p.129.

[7] R. Poduri and L.Q. Chen, Computer simulation of the kinetics of order-disorder and phase separation during precipitation of δ' (Al_3Li) in Al-Li alloys [J], *Acta Mater.*, 45(1997), No.1, p. 245.

[8] Y.Z. Wang, L.Q. Chen, and A.G. Khachaturyan, Strain-induced modulated structures in two-phase cubic alloys. [J], *Scripta Metall. Mater.*, 25(1991), No.8, p.1969.

[9] L. LÖchte, A. Gitt, G. I. Gottstein, *et al.*, Simulation of the evolution of GP zones in Al-Cu alloys: an extended Chan-Hilliard approach [J], *Acta Metall.*, 48 (2000), p.2972.

[10] V.G. Vaks, A.J. Larkin, C.A. Pikin, *et al.*, The elastic strain energy of coherent ellipsoidal precipitates in anisotropic crystalline solids [J], *Metall. Trans.*, 8A(1977), p.963.

[11] R.W. Cahn, P. Haasen, and E.J. Kramer, Phase Transformations in Materials [M] (in Chinese), Science Publish Press, Beijing, 1998, p.125.

[12] Y.D. Tyapkin, I.V. Gongadze, Y.I. Maliyenko, Structural Mechanism of coalescence of aging Ni-Cu-Si alloys [J], *Phys. Met. Metall.*, 66(1988), p.160.